

Numerical Investigation of Influence of Microbubble Injection, Distribution, Void Fraction and Flow Speed on Frictional Drag Reduction



Sudhir Sindagi, R. Vijayakumar, Somanath Nirali and B. K. Saxena

Abstract The increase in fuel costs and looming restrictions on carbon dioxide emissions are driving the shipowner into reducing the ship's resistance and required installed power. It was earlier reported that, merchant vessels operating at lower speeds, the frictional drag accounts of almost 70–80% of the total drag; thus, there is a strong demand for the reduction in the fluid frictional drag, especially in the marine transportation business. The use of air as a lubricant, by injecting below the plate or the body, which is famously known as microbubble drag reduction (MBDR) in order to reduce that frictional drag is an active research topic. Latest developments in this field suggests that there is a potential reduction of 80% in frictional drag in case of flat plates and about 30% reduction in case of ships, which encourages researchers to investigate further. In this study, 3D numerical investigations into frictional drag reduction by microbubbles were carried out in Star CCM+ on a channel for different flow velocities, different void fractions and different cross sections of flow at the injection point. This study is the first of its kind in which variation of coefficient of friction both in longitudinal and transverse directions was studied along with actual localized variation of void fraction at these points. The numerical framework consists of the Reynolds-averaged Navier–Stokes (RANS) equations and the standard $k-\varepsilon$ turbulence model with standard wall function treatment, which is validated in both conditions of with and without microbubbles with the existing experimental data. The design exploration study was carried out for various flow speeds, injector flow rates, cross sections of the channel/heights of channels and of

S. Sindagi (✉) · S. Nirali · B. K. Saxena
Tolani Maritime Institute, Pune, India
e-mail: sindagi@gmail.com

S. Nirali
e-mail: somnathnirali@gmail.com

B. K. Saxena
e-mail: brjendras@tmi.tolani.edu

R. Vijayakumar
Indian Institute of Technology Madras, Chennai, India
e-mail: vijay2028@iitm.ac.in

course void fractions. Coefficient of friction and void fraction values are measured at 12 longitudinal positions, and at each longitudinal position, 11 in number transverse and 10 in number depthwise positions were studied. In all, for one simulation, data at more than 1000 positions were collected. More than 60 simulations were carried out to understand the effect. From the study, it is concluded that since it is a channel flow and as the flow is restricted in confined region, effect of air injection is limited to smaller area in transverse direction as bubbles were not escaping in transverse direction.

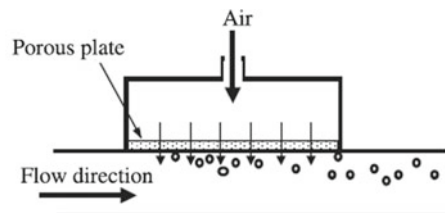
Keywords MBDR · Microbubbles · Frictional drag reduction

1 Introduction

Vehicles moving in water experience more frictional drag than vehicles on land or in the air, as the viscosity of water is higher than that of air. The increase in fuel costs and looming restrictions on emissions are driving the shipowner into reducing the ship's resistance and required installed power. It is reported that the fluid frictional drag accounts for as much as 60% of the total drag for cargo ship, and about 80% of that for a tanker; thus, there is a strong demand for the reduction in the fluid frictional drag. Numerous technologies [1], such as use of the micromorphology riblets, use of polymers, use of heating wall and vibrating the flexible wall, partial cavity creation, antifouling and coatings and super-hydrophobic surface and MBDR, have been studied and utilized to reduce the frictional drag of a surface. As shown in Fig. 1, MBDR effect is realized by injecting gas or air below the moving object (plate, ship, etc.).

This leads to two distinct drag-reducing phenomena: the bubble drag reduction and the air layer drag reduction. Experimental results of the air bubble drag reduction show that a significant drag reduction of greater than 25% could be made in the first few metres downstream of injection, and by gas layer formed on the underside of the flat plate, reduction of greater than 80% was measured. It is concluded that, MBDR has added advantages over other drag-reducing technologies, such as environmental-friendly, easy operation, low costs and high saving of energy. It is also reported that the MBDR is able to achieve 80% reduction in frictional drag, which can result in

Fig. 1 Schematic drawing of a microbubble injecting system



a substantial fuel savings for both commercial and naval ships. The most significant contribution regarding microbubble drag reduction was presented McCormick and Bhattacharyya [2] by demonstrating hydrogen bubbles generated by electrolysis to reduce frictional drag on a fully submerged body of revolution. Experimental studies [3–7] on flat plate have been carried out to understand the effect of air lubrication on reduction of drag. Numerical simulation/numerical model of MBDR [4, 8–17] for the flat plate has been developed to understand the effect, while similar studies on the ship model [18–24] have been carried out. Numerical model employed in the investigation comprises of a microbubble laden flow, wherein two independent sets of Reynolds-averaged Navier–Stokes (RANS) transport equations were used to describe both phases of the flow. The shear stress transport (SST) turbulence model or a standard $k-\omega$ turbulence model were used as the turbulent closure for the primary phase, and a zero-equation turbulence model is used for the microbubbles. Multiple-size group (MUSIG) based on population balance models, which resolves a wide range of bubble sizes taking into account the bubble break-up and coalescence, has been used [10] for the simulation.

In this study, numerical investigations into frictional drag reduction by microbubbles were carried out in a channel for different flow velocities, different void fractions and different cross sections of flow at the injection point. This study is the first of its kind in which variation of coefficient of friction both in longitudinal and transverse directions was studied along with actual localized variation of void fraction at these points. The numerical framework consists of the Reynolds-averaged Navier–Stokes (RANS) equations and the standard $k-\varepsilon$ turbulence model with standard wall function treatment, which is validated in both conditions of with and without microbubbles by the existing experimental data. These simulations were aimed at understanding the mechanism of resistance reduction. Flow parameters were changed by changing the pressure and/or velocity of flow at the injector location by changing the depth of channel at the point of injection. The influence of bubble distribution near a wall, which directly controls the void fraction, was also investigated. The design exploration study was carried out for various flow speeds, injector flow rates, cross sections of the channel/heights of channels and of course void fractions.

2 Numerical Set-up and Validation with Experimental Results

2.1 *Enhancements Over Experimental Investigation Using CFD*

The experimental study was conducted by [25] using recirculating water channel shown in Fig. 2. The test section, which is 10 mm high, 100 mm wide and 2000 mm long, generates a fully developed turbulent flow. Compressed air was injected into the channel for different flow rates, and its effect was measured using shear stress

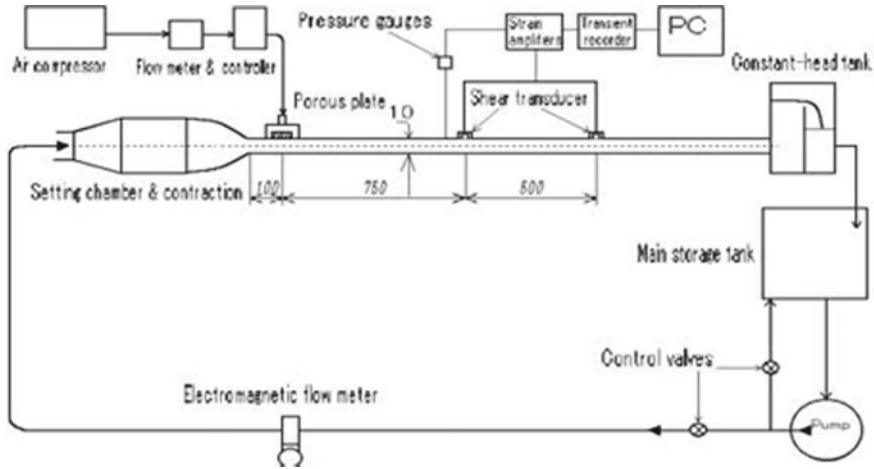


Fig. 2 Experimental set-up used for the investigation of MBRD by Moriguchi and Kato [25]

transducers placed at 750 and 1250 mm from the injection point. Similar set-up is used here to enhance the study using CFD technique. The experimental investigation was carried out at only two longitudinal locations, and no observation was made at spanwise locations, which is easily possible in CFD technique. In the numerical set-up, microbubbles were injected through series of holes of 1 mm in diameter in the test section at the upstream upper surface, generating air–liquid flow. Coefficient of friction and void fraction values were measured at 12 longitudinal positions, and at each longitudinal position, 11 in number transverse and depthwise positions were observed. In all, for one simulation, data at more than 1000 positions were collected. As shown in Table 1, simulations were performed at flow velocities ranging 4–7 m/s in the interval of 1 m/s, and at different airflow rates (12 values of void fraction). More than 60 simulations were carried out to study the effect of these flow parameters on coefficient of friction. Effect on C_F was also studied by changing the depth of channel at the injection point, which changes flow parameters. Here, as C_F values for different cases of injection of bubbles depend on the instance of time, they are normalized by averaging C_F values for time. In all, C_F value at one location is calculated by averaging their values for more than 1000 iterations, once the solution is converged.

Table 1 Flow velocities and void fractions for which simulations carried out along with positions at which C_F being calculated

Flow speed of water	Void fraction	Longitudinal positions of C_F being measured (mm)	Transverse positions of C_F being measured (on one side of CL) (mm)	Distance from wall (mm)
4	0.015	100	0	0
5	0.03	200	1	1
6	0.045	350	2	2
7	0.06	400	3	3
	0.075	500	4	4
	0.09	600	5	5
	0.105	700	-1	6
	0.115	750	-2	7
	0.135	800	-3	8
	0.14	900	-4	9
		1000	-5	10
		1250		

2.2 Grid Independency Study and Numerical Set-up

The numerical and mesh set-up used for this exhaustive study is shown in Figs. 3 and 4. Grid independency study was also carried out to optimize and finalize the meshing. Initially, uniform mesh was generated throughout the channel, which, based on flow regime of air bubbles, is optimized for the further study. Dense meshing was generated for both with and without injection of air till no change in final result is obtained. Optimized mesh is shown in Fig. 4. For the simulation of three-dimensional, implicit unsteady segregated flow, volume of fluid (VOF) approach was used to solve Reynolds-averaged Navier–Stokes (RANS) equations and Eulerian multiphase equations of state with multiphase interactions based on density and surface tension of air and water. To account for the boundary layer effect, exact wall distance, two layer all y^+ wall treatment and realizable K-epsilon two-layer approaches were effectively utilized. For the simulation of turbulence, K-epsilon turbulence model was used. Velocity inlet boundary condition was used to set up the flow velocity of water at water inlet boundary. Similarly, for setting up of air inlet, mass flow rate boundary condition was used. At the outlet, pressure outlet boundary condition is used. For all other sides of channel, typical wall boundary condition with no slip condition was used.

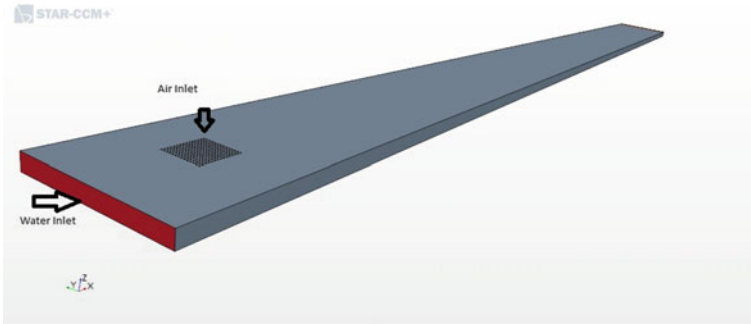


Fig. 3 Geometry used for simulations

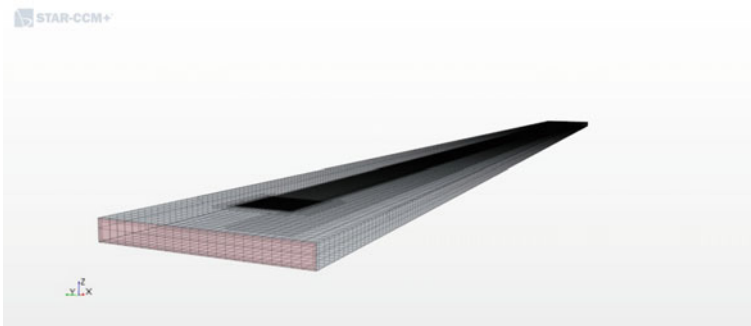


Fig. 4 Optimized mesh used for simulations

2.3 Validation of CFD Results with Experimental Results

Figure 5 shows the comparison of C_{F0} values with experiment without injection of air at a location of 750 mm from the injection point. Moreover, Figs. 6, 7 and 8 show the comparison of reduction in C_F values with experimental values, with and without injection of air at flow speed of 5, 6 and 7 m/s, respectively. Here, C_{F0} refers to the coefficient of friction without the injection of bubbles and C_F refers to coefficient of friction with the injection of bubbles. The value of C_F is calculated using

$$C_F = \frac{\tau_w}{\frac{1}{2}\rho_m U_m^2}$$

where τ_w —shear stress, ρ_m —mean density of flow and U_m —mean flow velocity.

It is the general practice to show reduction in friction drag against the void fraction or volume fraction represented as

$$\text{Void Fraction or Volume Fraction (VF)} = \frac{Q_a}{Q_a + Q_w}$$

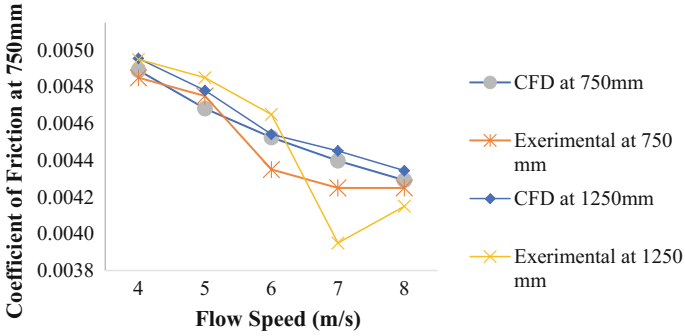


Fig. 5 Comparison of C_F values with experiment, without injection of air

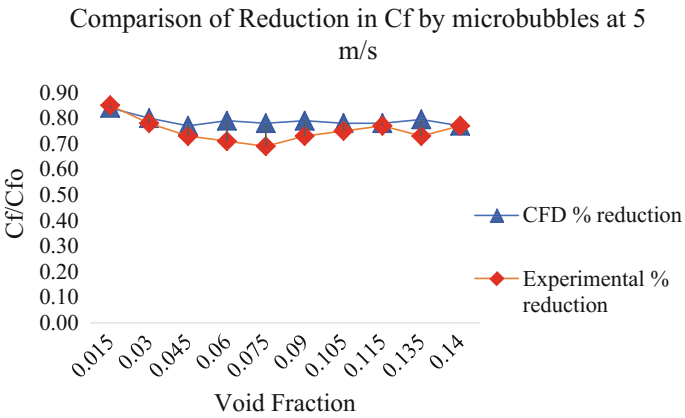


Fig. 6 Comparison of reduction in C_F with experiment, with and without injection of air at flow speed of 5 m/s

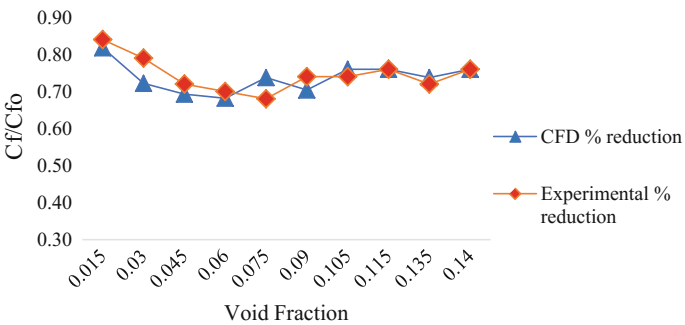


Fig. 7 Comparison of reduction in C_F with experiment, with and without injection of air at flow speed of 6 m/s

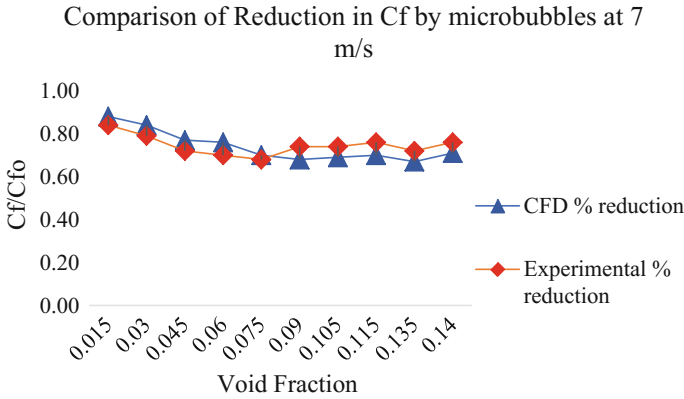


Fig. 8 Comparison of reduction in C_F with experiment, with and without injection of air at flow speed of 7 m/s

where Q_a —air injection rate and Q_w —water flow rate.

From the comparison made, it can be seen that the simulation results obtained match closely with experimental results. Moreover, due injection of air below the plate causes reduction in the frictional drag. Reduction obtained depends on many factors such as void fraction, flow speed and location of point of analysis from the injection point. From these figures, it can be concluded that maximum reduction obtained due to injection of microbubbles is 33%, which also matches with experimental results.

3 Results and Discussion

3.1 Investigation of Alteration of Flow Parameters Due to Injection of Microbubbles

Frictional drag of any body is given by the expression

$$R_F = C_F \frac{1}{2} \rho S V^2$$

From the above expression, it can be concluded that to reduce the frictional drag, one must reduce C_F , density of liquid (ρ) flowing and the wetted surface area (S). As seen from the previous experiments based on MBDR, it is clearly mentioned that combined effect of reduction in density and wetted surface area along with reduction in C_F due to alteration of flow properties and modification of turbulent momentum transport due to the presence of bubbles causes considerable reduction in frictional

drag. When air is injected into the boundary layer, an air–water mixture flow containing both air bubbles and water can be formed. If the amount of injected air increases, air bubbles begin to coalesce into patches that cover the surface continuously, and a transitional air layer is formed, where the patches coexist with air bubbles. If the flow rate of air is further increased, a continuous layer of air layer is formed, reducing the direct contact of water with the surface. Formation of continuous layer of air is the ultimate thing, reducing density of fluid from water to air. As observed from Fig. 9, the density variation is plotted against time at a location of 750 mm from the injection point. From Fig. 9, it can be concluded that the reduction in density is almost of the order of 45% which is causing the reduction in frictional drag. The shear stress developed due to viscosity of liquid can be estimated by using

$$\tau_w = \mu \frac{du}{dy} - \rho U' V'$$

However, $U' V' = -q \Lambda \frac{\partial u}{\partial y}$

By substitution, we get

$$\tau = (\mu + \rho q \Lambda) \frac{\partial u}{\partial y}$$

where $q \Lambda$ is eddy viscosity, q^2 is turbulence energy, and Λ is energy containing turbulent scale. This shows that microbubble drag reduction is the result of three factors: reduction of density, increase of bubble suspension viscosity as the concentration approaches the packing limit and turbulence modification of the boundary layer. When air bubbles are present, the density of mixture decreases and accordingly shear stress is reduced. The second term in the above equation is known as Reynolds stress, which reduces as the density (ρ) decreases. From Figs. 10 and 11, it can be concluded that the reduction in turbulent viscosity, dynamic viscosity at the

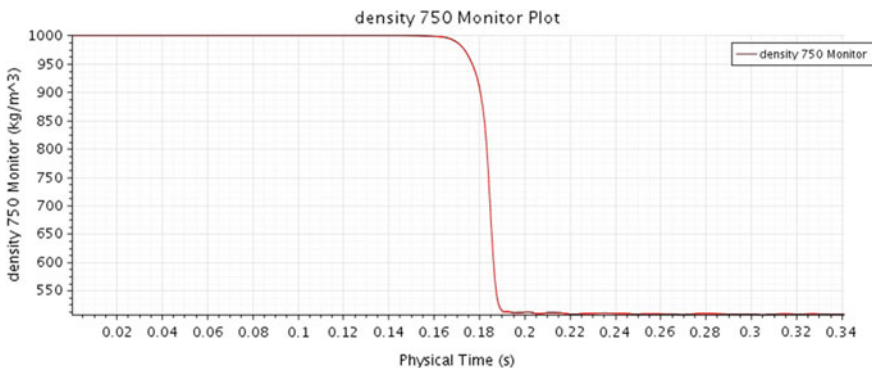


Fig. 9 Variation of effective density of flow at 750 mm with respect to time at flow speed of 5 m/s and void fraction of 0.035

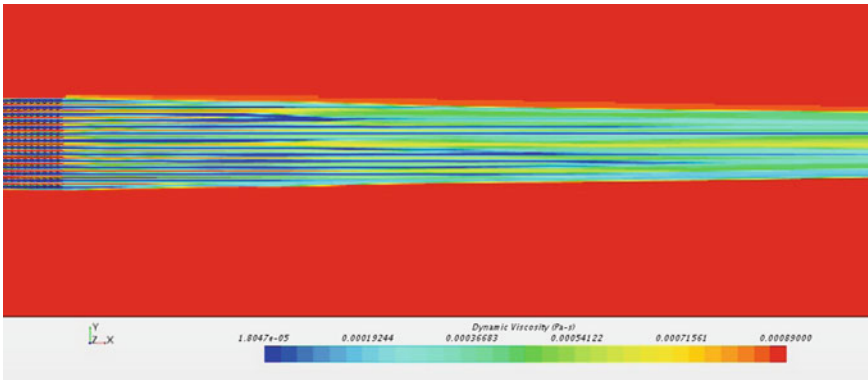


Fig. 10 Variation of dynamic viscosity at flow speed of 6 m/s and void fraction of 0.105

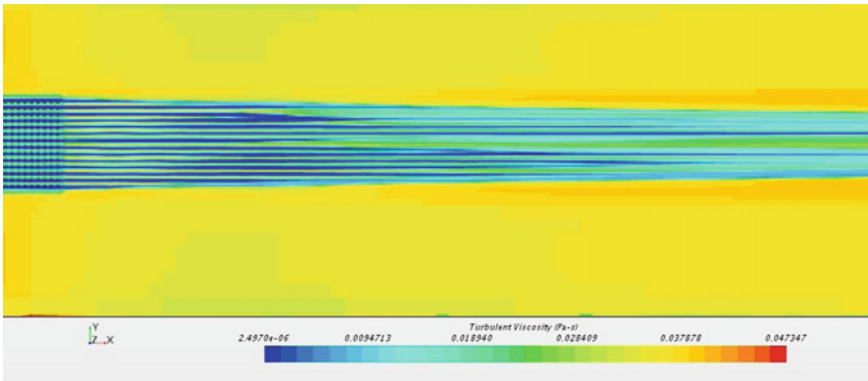


Fig. 11 Variation of turbulent viscosity at flow speed of 6 m/s and void fraction of 0.105

localized area along with reduction in density due to injection of microbubbles, is causing reduction in C_F values.

Similarly, as presented in Figs. 12 and 13, other reasons for the reduction in the frictional drag are reduction in turbulent viscosity and increase in the turbulence dissipation rate due to the injection of bubbles. Reduction in density along with reduction in turbulent viscosity and increase in the turbulence dissipation rate are causing reduction in the frictional drag.

To conclude, MBDR effect is due to the alteration of local effective viscosity and density of the fluid along with the increase in turbulence dissipation rate reduces the Reynold's stress and in turn reduces the shear stress.

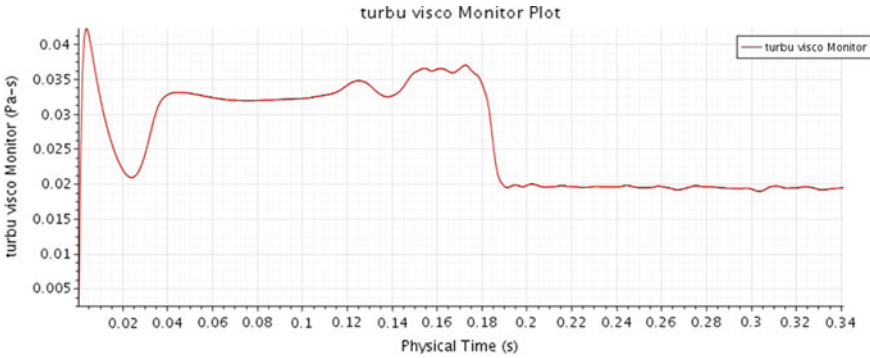


Fig. 12 Variation of turbulent viscosity at 750 mm with respect to time at flow speed of 5 m/s and void fraction of 0.035

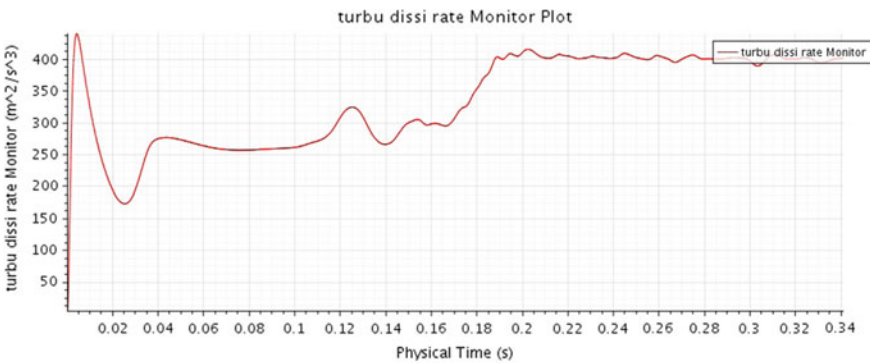


Fig. 13 Variation of turbulence dissipation rate at 750 mm with respect to time at flow speed of 5 m/s and void fraction of 0.035

3.2 Study at Flow Speed of 6 m/s at Different Void Fractions

Figures 14 and 15 describe the variation of C_F values in longitudinal and transverse directions for two values of void fractions of 3 and 10.5%. From these figures, it can be concluded that with the increase in distance from the injection point in the longitudinal direction, C_F value increases, which is a general trend observed in many experiments. It means that the MBDR effect reduces with the increase in distance from the injection point. The transverse variation of MBDR effect is also observed very closely in the simulation. From these simulation results, it can be concluded that C_F value reduces with the increase in transverse distance from the centre line of channel. This reconfirms that MBDR effect reduces with the distance from the injection point both in longitudinal and transverse directions. Moreover, from Figs. 16 and 17, it can be seen that injected air converges to a smaller area in the transverse direction. This is in fact due the effect of boundary layer formation

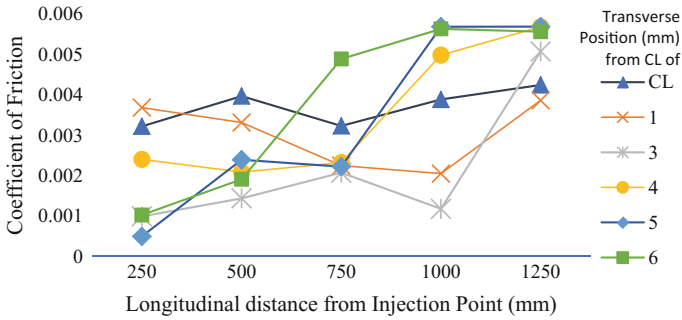


Fig. 14 Variation of C_F for flow speed of 6 m/s and volume fraction of 0.03

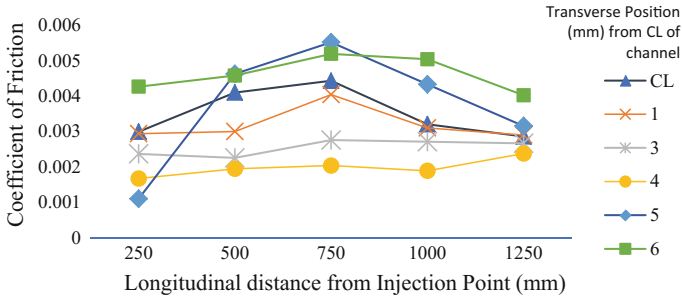


Fig. 15 Variation of C_F for flow speed of 6 m/s and volume fraction of 0.105

from side plates of channel. Hence, in case of rectangular channel, the MBDR effect is limited to smaller area in transverse direction. This clarifies that unlike in case of free flow to the sideways, wherein the bubbles escape in sideways, the bubbles are restricted to move in smaller area. Similar observation is made in Fig. 15, wherein C_F value increases with the distance from centre line of channel and it is maximum at a distance of 6 mm from the centre line. Interesting observation has been made from Fig. 15 that C_F value reduces after 750 mm from the injection point. This may be due to the fact that since bubbles are not escaping from the sides and as they are converging to smaller area of flow, possibly this concentration of bubbles is causing further reduction in C_F values. Similar conclusion can be made from Fig. 14.

Figure 17 also depicts that as the distance increases in the longitudinal direction, bubbles coalesce with each other and form air pockets. This is the major reason for variation in C_F values in longitudinal direction, as bubbles coalesce to form air pockets avoiding any contact of water with the surface and thus reducing the coefficient of friction. Figure 18 describes the longitudinal variation of C_F values for different values of void fraction. From Fig. 18, it can be concluded that C_F value decreases till void fraction is of 7.5%, beyond which these values start increasing. This may be due to the additional turbulence created by the injection of air bubbles.

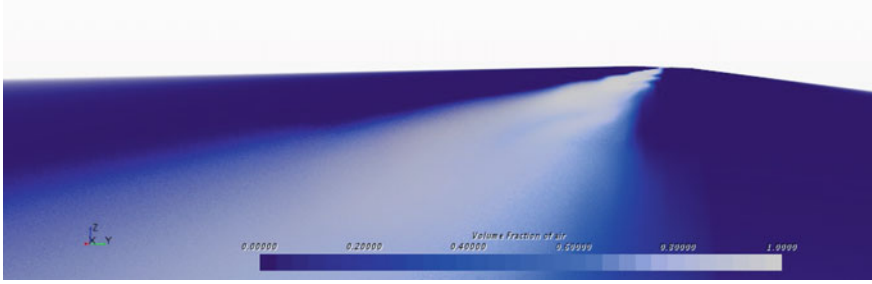


Fig. 16 Variation of volume fraction of air both in transverse and longitudinal directions

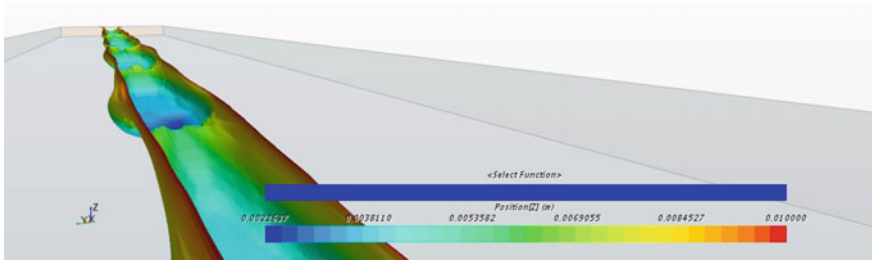


Fig. 17 Variation of volume fraction of air both in all directions

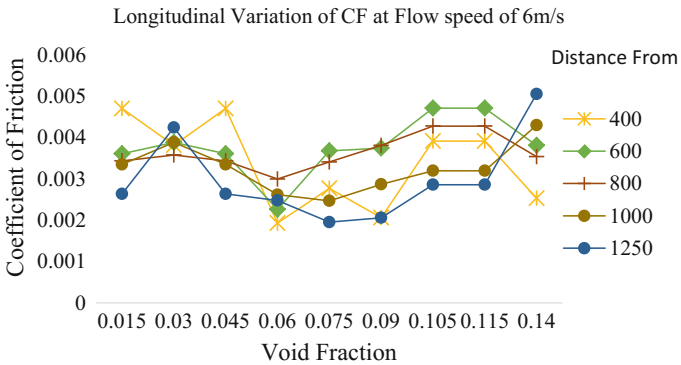


Fig. 18 Longitudinal variation of C_F at flow speed of 6 m/s and different void fraction

To conclude, as the MBDR effect depends upon the presence of microbubbles, C_F values keep varying from point to point and do not follow any particular pattern.

Figure 19 describes variation of C_F values at different longitudinal and transverse locations for flow speed of 6 m/s and VF 11.5%, which clearly shows that C_F values increase with the increase in longitudinal and transverse distances from the air injection point. Moreover, it can be seen that there is a variation in C_F values in

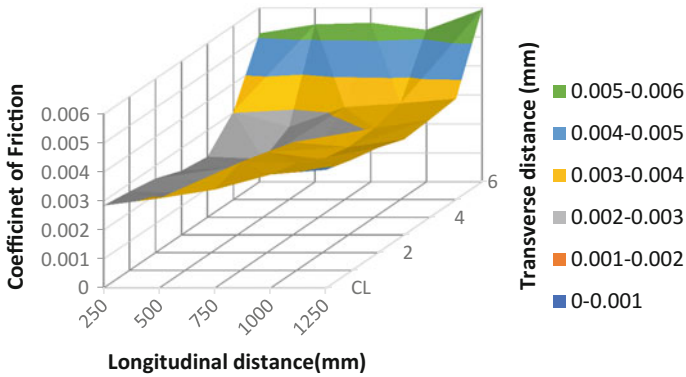


Fig. 19 Variation of C_F at different longitudinal and transverse locations at flow speed of 6 m/s and VF 11.5%

longitudinal direction, which is mostly due to coalescence and breaking of bubbles with the distance from the injection point.

3.3 Study at Flow Speed of 5 m/s at Different Void Fractions

As mentioned earlier, investigation of MBDR effect was carried out at 5 m/s. From Fig. 20, it can be concluded that MBDR effect reduces with its distance from the injection point. Increase in effect at location 1250 mm from the injection point is due to the concentration of air bubbles at the location. As shown in Fig. 21 and similar to observation made at flow speed of 6 m/s, MBDR effect reduces with the increase in distance from the injection point in transverse direction. Investigation of MBDR effect in longitudinal direction along with variation of void fraction clarifies that for the void fraction value of 2%, where injection rate is very low, MBDR effect is low. With the increase in void fraction, MBDR effect increases, reaches to maximum and then further reduces. This may be due to the increase in turbulent viscosity caused due to the additional momentum created by injection of bubbles in the flow at higher rate.

To conclude, the distance from the injection point is the most important parameter in obtaining the reduction in frictional drag and that the boundary layer thickness of top plate has little effect on the skin friction reduction by microbubbles.

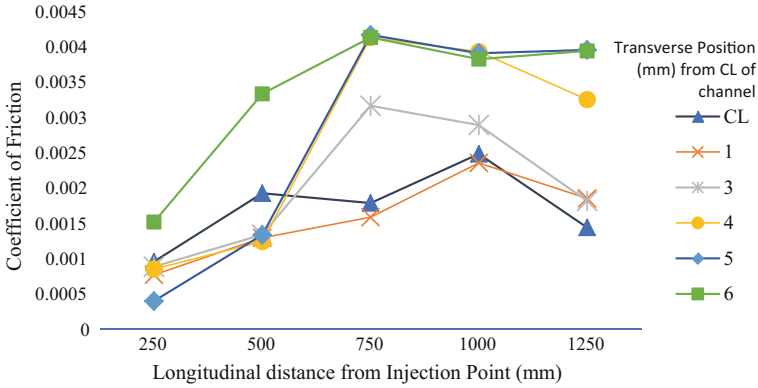


Fig. 20 Variation of C_F for flow speed of 5 m/s and volume fraction of 0.035

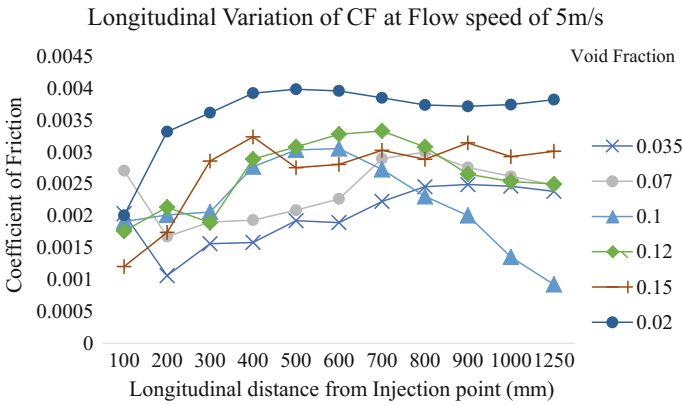


Fig. 21 Longitudinal variation of C_F at flow speed of 5 m/s and different void fraction

3.4 Study at Flow Speed of 7 m/s at Different Void Fractions

Figure 22 represents the variation of C_F values in longitudinal and transverse directions for flow speed of 7 m/s at void fraction of 9%. Interesting conclusion can be made from these results. Maximum MBDR effect occurs at a distance of 3 mm from the centre line and not at the centre line. Of course, the effect reduces with distance from the centre line. Figure 23 represents the variation of C_F values in longitudinal direction for flow speed of 7 m/s at different values of void fraction. From the figure, it can be concluded that MBDR effect is maximum at void fraction of 6%. The effect is minimum at void fraction of 3%, reaches to maximum value at 6% and again reduces at 9%. This implies that MBDR effect does not increase with the increase in airflow rate. At higher injection rate, it increases the turbulence of the flow, which alters the flow parameters increasing the frictional drag. In other words, to conclude,

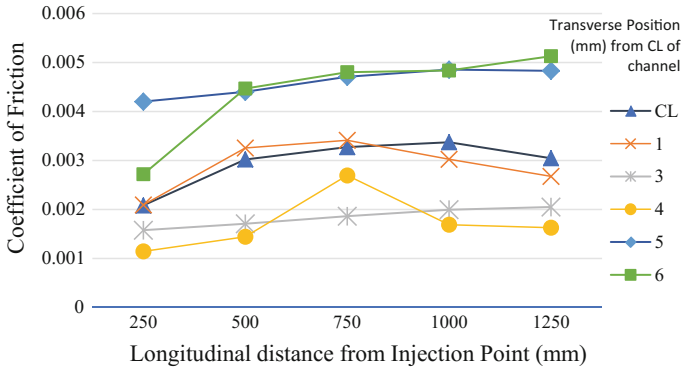


Fig. 22 Variation of C_F for flow speed of 7 m/s and volume fraction of 9%

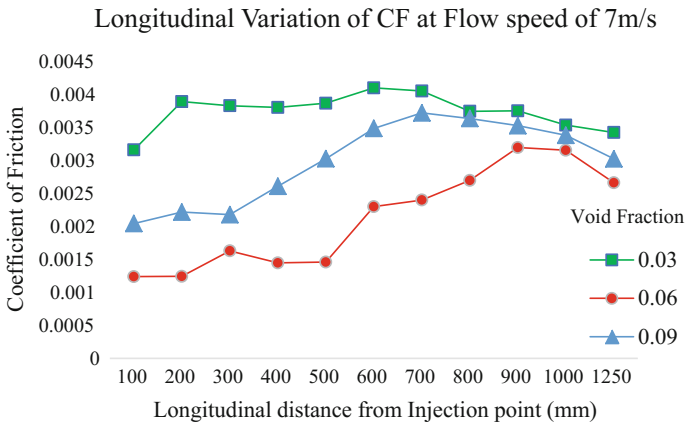


Fig. 23 Longitudinal variation of C_F at flow speed of 7 m/s and different void fraction

excessive microbubble injection destroys the favourable turbulent boundary layer and in doing so decreases the drag reduction effect.

3.5 Variation of C_F Values in the Longitudinal Direction for Different Speeds and VF

Investigation on effect of flow speed on MBDR effect in longitudinal direction for different void fractions was carried out. From Figs. 24 and 26, it can be concluded that for void fraction values of 3 and 9%, in general, MBDR effect is more for a flow speed of 5 m/s giving lowest values of coefficient of friction. However, as shown in Fig. 25, in general, MBDR effect was found to be maximum at higher speed of

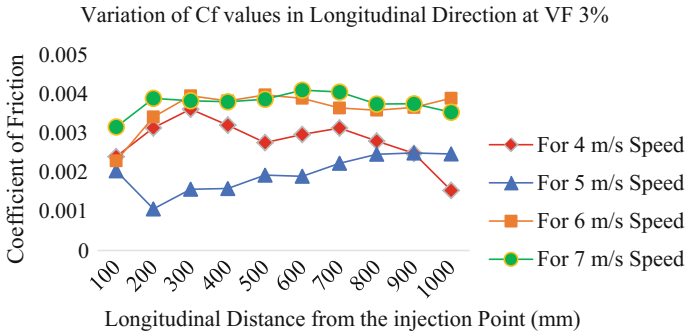


Fig. 24 Variation of C_F values in longitudinal direction for different flow speeds at VF of 3%

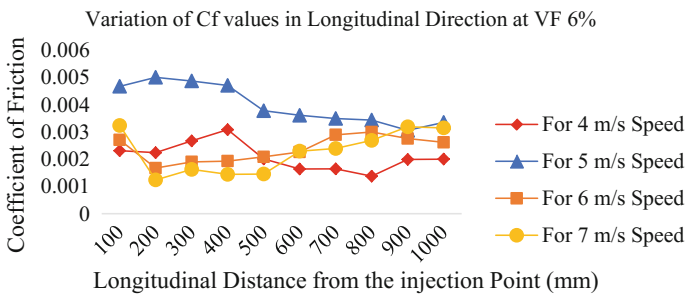


Fig. 25 Variation of C_F values in longitudinal direction for different flow speeds at VF of 6%

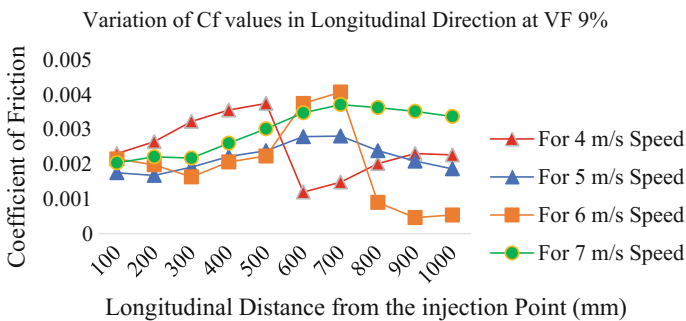


Fig. 26 Variation of C_F values in longitudinal direction for different flow speeds at VF of 9%

7 m/s at void friction of 6%. In most of the cases, MBDR effect reduced with the increase in distance from the injection point, except for few cases at void fraction of 9%, wherein MBDR effect increased from a point having distance 800 mm onwards for speed of 7 m/s and 600 mm onwards for 4 m/s.

To conclude, MBDR effect mostly depends on local void fraction than the injection void fraction. As mentioned previously, local void fraction depends on the coales-

cence and breaking of bubbles. Formation of air pockets increases the local void fraction and in turn reduces coefficient of fraction, which has been found in many cases, wherein MBDR effect was found to be more after certain distance from the injection point.

3.6 Variation of C_F Values in Transverse Direction for Different Speeds and VF

Similar investigation on effect of flow speed on MBDR effect in transverse direction for different values of void fraction was carried out. From Figs. 28 and 29, it can be concluded that for void fraction values of 6 and 9%, MBDR effect reduced with the increase in distance from the injection point. For the case at void fraction of 3% (Fig. 27), similar observation was made for lower speeds of 4 and 5 m/s. However, at higher speeds, due to more turbulence created, air bubbles distributed more in spanwise direction, causing the increase in MBDR effect in spanwise direction. Moreover, MBDR effect is found to be more at lower speed of 4 m/s for VF 6%; however, for other cases of VF, similar trend could not be obtained, which implies that MBDR effect solely depends on local void fraction.

To conclude, MBDR effect quickly reduces in the streamwise direction at immediate downstream of injection and gradually decreases further downstream. In the spanwise direction, there is no constant reduction region and the reduction effect reduces linearly towards the side end.

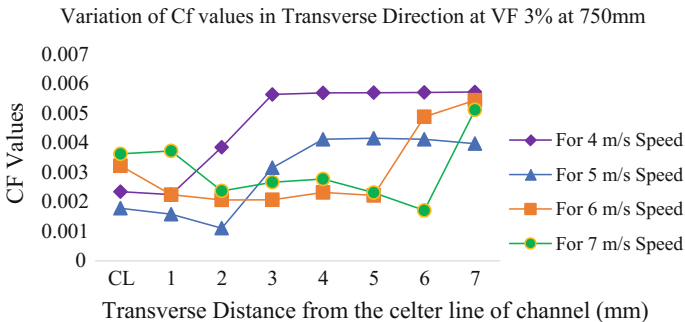


Fig. 27 Variation of C_F values in transverse direction for different flow speeds at VF of 3%

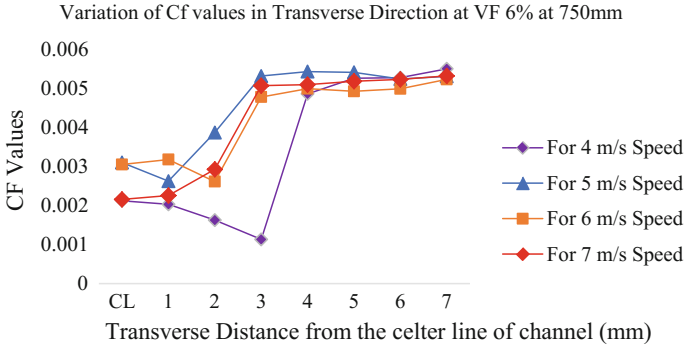


Fig. 28 Variation of C_F values in transverse direction for different flow speeds at VF of 6%

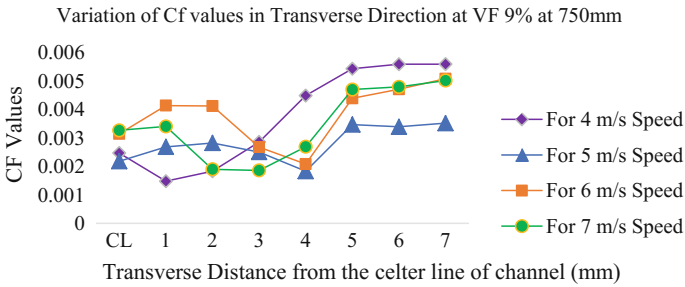


Fig. 29 Variation of C_F values in transverse direction for different flow speeds at VF of 9%

3.7 Investigation of Alteration of Flow Parameters and C_F Values for Different Depths of Channel at the Injection Point

It is well-known fact that diameters of microbubbles generated depend on the flow parameters at the injection point. Hence, to investigate this effect, three different channels have been studied. All three channels have the same test section height of 10 mm throughout the length except at the injection point. Channel 1 has an air injection channel height of 10 mm at the injection point, Channel 2 has an air injection channel height of 5 mm at the injection point, and Channel 3 has an air injection channel height of 20 mm at the same point. Channels 2 and 3 are shown in Fig. 30 along with velocity distribution throughout the length. Investigation has been carried out to check the changes in MBDR effect due to this variation in flow parameters for three different speeds of 5, 6 and 7 m/s at constant volume fraction of 6%.

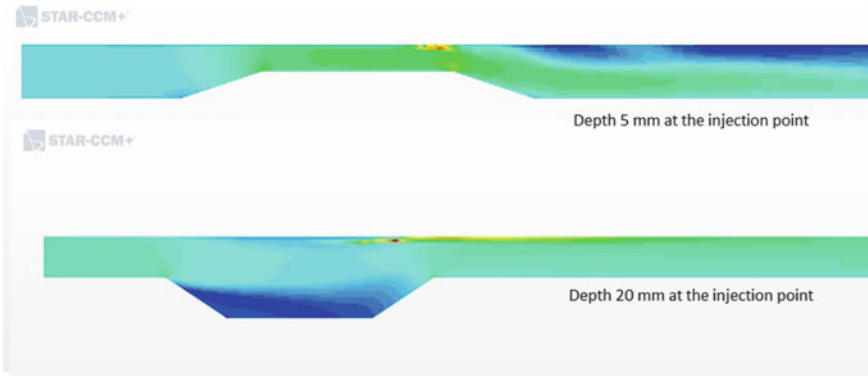


Fig. 30 Channels 2 and 3 with velocity distribution

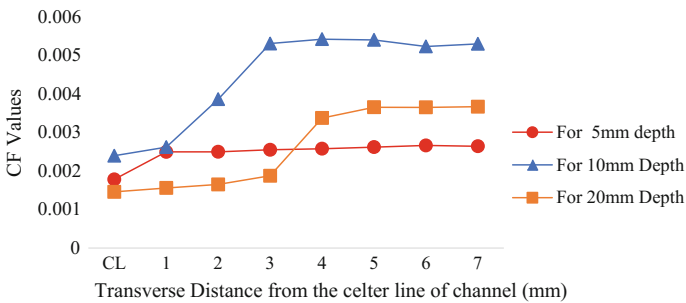


Fig. 31 Variation of C_F values in transverse direction at VF 6% at 750 mm and at flow speed of 5 m/s for different depths of channel

Figures 31, 32 and 33 show the variation of C_F values in transverse direction at 750 mm from the injection point and at constant value of volume fraction of 6% for different flow speeds of 5, 6 and 7 m/s, respectively, of course for different depths of channel. From these figures, it can be safely concluded that 5 mm depth at the injection point gives best results for the MBDR effect, attaining minimum values of coefficient of friction. Moreover, it can be seen that for 5 mm depth of channel, MBDR effect is almost equal in transverse direction. Also, it can be observed that MBDR effect is maximum for lower flow speed of 5 m/s as compared to other speeds. At higher flow speeds, additional turbulence created increases the turbulent viscosity and in turn the Reynolds stress.

Figures 34, 35 and 36 show the variation of C_F values at 750 mm in longitudinal direction at volume fraction of 6% and at flow speed of 5, 6 and 7 m/s, respectively, for different depths of channel. From these figures, it can be concluded that since bubbles are widely spreading in the transverse direction for 5 mm depth, MBDR effect in longitudinal direction reduces with the distance from the injection point. Moreover, the MBDR effect depends on both the flow speed and depth of channel at

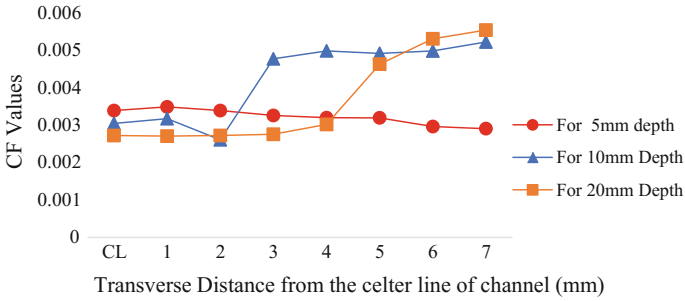


Fig. 32 Variation of C_F values in transverse direction at VF 6% at 750 mm and at flow speed of 6 m/s for different depths of channel

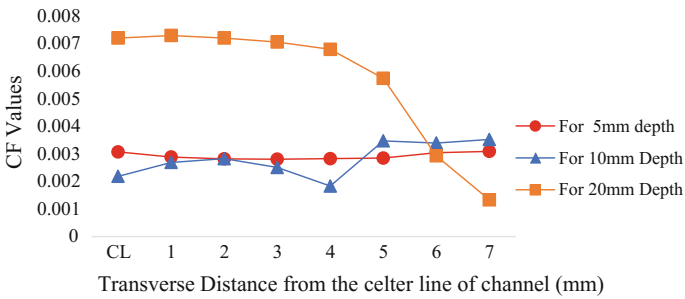


Fig. 33 Variation of C_F values in transverse direction at VF 6% at 750 mm and at flow speed of 7 m/s for different depths of channel

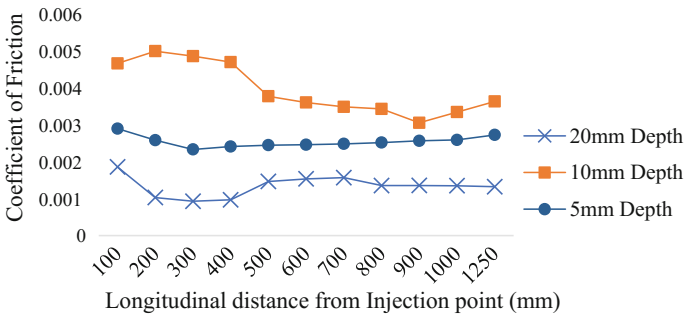


Fig. 34 Variation of C_F values in longitudinal direction at VF 6% at 750 mm and at flow speed of 5 m/s for different depths of channel

the injection point. As seen from the figures, for flow speed of 5 m/s, 20 mm depth of channel at the injection point gives best result; however, for flow speed of 6 m/s, 10 mm depth gives best results. This once again implies that MBDR effect depends solely on distribution of bubbles which controls the local void fraction.

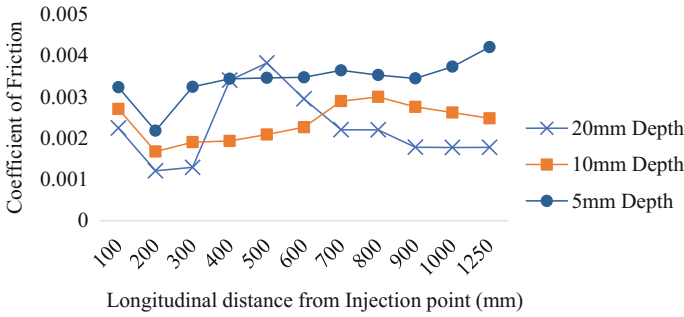


Fig. 35 Variation of C_F values in longitudinal direction at VF 6% at 750 mm and at flow speed of 6 m/s for different depths of channel

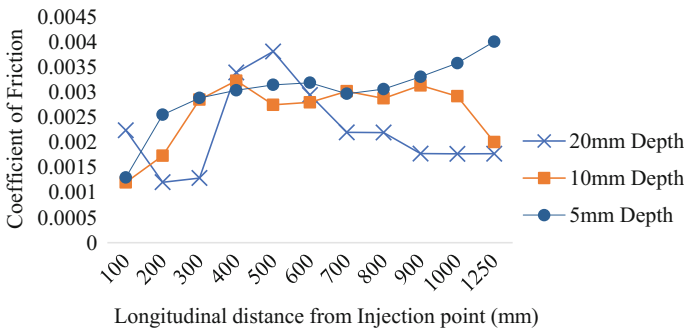


Fig. 36 Variation of C_F values in longitudinal direction at VF 6% at 750 mm and at flow speed of 7 m/s for different depths of channel

Figure 37 shows the variation of void fraction and in turn distribution of microbubbles for different depths of channel at the injection point. As seen from the figure, for 5 mm depth of the channel, due to reduction of pressure at the injection point, flow velocity increases which in turn causes the increase in turbulence. This is forcing microbubbles to widely distribute in transverse direction and giving equal reduction in frictional drag in the transverse direction as well. Moreover, the flow rate in longitudinal direction decreases due to reduction in depth. To balance the mass flow rate, air volume fraction increases in spanwise direction. In case of depth of 10 mm or more, since velocity in longitudinal direction is less at the injection point as compared to 5 mm depth of channel, distribution of air bubbles in the spanwise direction is confined to smaller area.

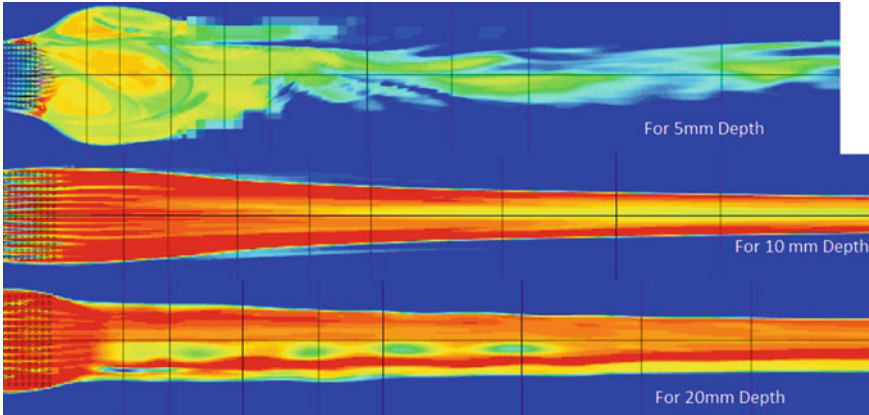


Fig. 37 Variation of void fraction for different depths at the injection point

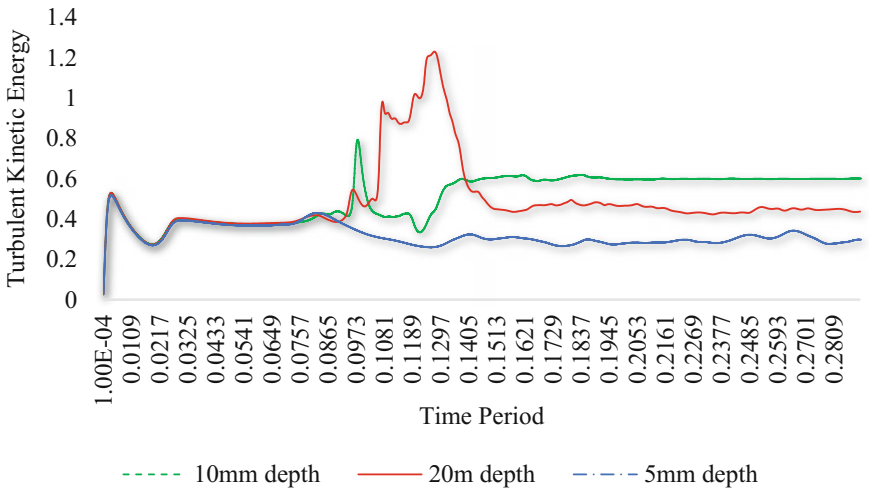


Fig. 38 Variation of turbulent kinetic energy for different depths at 750 mm from the injection point

Figure 38 depicts the variation of turbulent kinetic energy for different depths at 750 mm from the injection point. From the distribution, it is confirmed that for 5 mm depth of channel, as more number of bubbles are distributed in spanwise direction, turbulent kinetic energy reduces, and for 20 mm depth of channel, the same is increased due to the injection of air. Moreover, from Fig. 38, it can be concluded that turbulent kinetic energy is lesser for 5 mm depth of channel. This implies that out of three channels tested, channel with depth of 5 mm gives the best results to reduce the frictional drag.

To conclude, it is found that the most important parameter in determining the fraction of drag reduction during gas injection is the effective void fraction, which is influenced by both—the injection rate and the static pressure under the test conditions.

4 Conclusions

The effect of microbubbles on frictional drag reduction was investigated in a 3D turbulent flow channel, with the main aim of investigating the effect of flow speed, void fraction and geometry at the injection point. Coefficient of friction and void fraction values are measured at 12 longitudinal positions, and at each longitudinal position, 11 in number transverse and 10 in number depthwise positions were studied. In all, for one simulation, data at more than 1000 positions were collected. More than 60 simulations were carried out to understand the effect. From the study, it is concluded that:

- The most important parameter in deciding the MBDR effect is the effective void fraction at the point of analysis, which is influenced by both—the injection rate and the static pressure under the test conditions. The reduction in the frictional drag is increased with the increasing mean void fraction.
- MBDR effect is due to the alteration of local effective viscosity and density of the fluid which reduces the Reynold's stress and in turn reduces the shear stress.
- Due to the restriction of flow in the spanwise direction, the MBDR effect reduces slowly in the streamwise direction and quickly reduces in the spanwise direction. The major reason for the same is distribution of air bubbles converging to smaller area in the spanwise direction as bubbles were not escaping sideways.
- The distance from the injection point is the most important parameter in obtaining the reduction in frictional drag, and the boundary layer thickness on the upper plate has little effect on the skin friction reduction by microbubbles.
- MBDR effect does not increase with the increase in airflow rate. At higher injection rate, excessive microbubble injection destroys the favourable turbulent boundary layer and in doing so decreases the drag reduction effect.
- MBDR effect depends on both the flow speed and depth of channel which decides the static pressure at the injection point.

Acknowledgements This research is well supported by SIEMENS Ltd. formerly known as CD ADAPCO. The authors express their sincere gratitude for their support. Moreover, the authors sincerely express their warm gratitude towards Mr. Sangmesh Biredar of CD ADAPCO for his invaluable inputs during the investigation using multiphase flow in Star CCM+.

References

1. Sindagi S, Vijaykumar R, Saxena BK (2016) Frictional drag reduction: an EFD and CFD based review of mechanisms. In: International conference on EFD and CFD—MARHY 2016, IIT Madras, India
2. McCormick M, Bhattacharyya R (1973) Drag reduction of a submersible hull by electrolysis. *Naval Eng J* 85:11–16
3. Fontaine AA, Deutsch S (1992) The influence of the type of gas on the reduction of skin friction drag by microbubble injection. *Exp Fluids* 13:128–136
4. Kanokjaruvijit K, Martinez-botas RF (2005) Jet impingement on a dimpled surface with different crossflow schemes. *Int J Heat Mass Transf* 48:161–170
5. Sanders WC, Winkel ES, Dowling DR, Perlin M, Ceccio SL (2006) Bubble friction drag reduction in a high-reynolds-number flat-plate turbulent boundary layer. *J Fluid Mech* 552:353–380
6. Elbing BR, Winkel ES, Lay KA, Ceccio SL, Dowling DR, Perlin M (2008) Bubble-induced skin-friction drag reduction and the abrupt transition to air-layer drag reduction. *J Fluid Mech* 612:201–236
7. Tsai J-F, Chen C-C (2011) Boundary layer mixture model for a microbubble drag reduction technique. *ISRN Mech Eng* 2011:9 (Article ID 405701)
8. Kim S-Y (1995) The persistence of drag reduction following the injection of microbubbles into a turbulent boundary layer. *Int Commun Heat Mass Transfer* 22(3):353–357
9. Lu J, Fernández A, Tryggvason G (2005) The effect of bubbles on the wall drag in a turbulent channel flow. *Phys Fluids* 17:095102
10. Mohanarangam K, Cheung SCP, Tu JY, Chen L (2009) Numerical simulation of micro-bubble drag reduction using population balance model. *Ocean Eng* 36:863–872
11. Skudarnov PV, Lin CX (2006) Drag reduction by gas injection into turbulent boundary layer: density ratio effect. *Int J Heat Fluid Flow* 27:436–444
12. Kim D, Moin P (2010) Direct numerical study of air layer drag reduction phenomenon over a backward-facing step. Centre for Turbulence Research Annual Research Briefs
13. Rzehak R, Krepper E (2013) CFD modelling of bubble-induced turbulence. *Int J Multiph Flow* 55:138–155
14. Madavan K, Deutsch S, Merkle CL (1985) Numerical investigations into the mechanisms of microbubble drag reduction. *Trans ASME* 107:370–377
15. Legner HH (1984) A simple model for gas bubble drag reduction. *Phys Fluids* 27:2788
16. Kanai A, Miyata H (2001) Direct numerical simulation of wall turbulent flows with microbubbles. *Int J Numer Methods Fluids* 35:593–615
17. Ceccio SL (2010) Friction drag reduction of external flows with bubble and gas injection. *Ann Rev Fluid Mech* 42:183–203
18. Wu C-S, He S-L, Zhu D-X, Gu M (2006) Numerical simulation of microbubble flow around an axisymmetric body. In: Conference of global Chinese scholars on hydrodynamics
19. Kawabuchi M, Kawakita C, Mizokami S, Higasa S, Kodan Y, Takano S (2011) CFD predictions of bubbly flow around an energy-saving ship with Mitsubishi air lubrication system. *Mitsubishi Heavy Ind Tech Rev* 48(1)
20. Davenport J, Hughes RN, Shorten M, Larsen PS (2011) Drag reduction by air release promotes fast ascent in jumping emperor penguins- a novel hypothesis. *Mar Technol Prog Ser* 430:171–182
21. Shereena SG, Vengadesan S, Idichandy VG, Bhattacharyya SK (2013) CFD study of drag reduction in axisymmetric underwater vehicles using air jets. *Eng Appl Comput Fluid Mech* 7(2):193–209
22. Zverkhovskiy O, Kerkvliet M, Lampe A, Vaz G, van Terwisgab T Numerical study on air cavity flows. MARIN
23. Lyu X, Tang H, Sun J, Wu X, Chen X (2014) Simulation of microbubble resistance reduction on a suboff model. *Brodogradnja/Shipbuilding* 65(2)
24. Dogrul A, Arikani Y, Celik F (2010) A numerical investigation of air lubrication effect on ship resistance

25. Moriguchi Y, Kato H (2002) Influence of microbubble diameter and distribution on frictional resistance reduction. *J Mar Sci Technol* 7:79–85